A HYBRID FINITE-ELEMENT/PARTICLE-SIMULATION METHOD FOR THE ANALYSIS OF SEMICONDUCTOR TRANSIENTS AND BIPOLAR TRANSPORT

R. C. MARTIN and N. M. GHONIEM

Mechanical, Aerospace and Nuclear Engineering Department, University of California,
Los Angeles, CA 90024-1597, U.S.A.

Abstract—A new method is introduced for the self-consistent transient solution of semiconductor device equations for both majority and minority carrier transport. An axisymmetric quadratic finite-element formulation is employed for the solution of the potential. The traditional conservation equations for the majority and minority carriers are replaced by equivalent equations for the drift motion and subsequent interactions of individual charged particles. Transport, recombination, and thermal generation processes are included. Drift forces on electrons and holes are computed from potential gradients. One-dimensional steady-state solutions obtained from transient evolution are compared to a fully iterative finite-element method for silicon diodes. Applications to axisymmetric device geometries are presented.

NOTATION

A, B	constants used in eqn (18) in text
$c_n(c_p)$	Auger electron (hole) recombination coefficient ($cm^6 s^{-1}$)
$D_n(D_p)$	electron (hole) diffusivity ($cm^2 s^{-1}$)
E	electric field ($V cm^{-1}$)
E_c	electric field parameter used in eqn (20) in text ($V cm^{-1}$)
G	carrier generation rate ($cm^{-3} s^{-1}$)
$J_n(J_p)$	electron (hole) current density ($A cm^{-2}$)
L_i	local shape function at node i
m	number of nodes in the computational mesh
n	electron carrier density (cm^{-3})
n_{int}	intrinsic carrier density (cm^{-3})
N_i	global shape function at node i
N_t	number of time intervals used in calculating the L-2 error norm
N_x	number of grid points used in calculating the L-2 error norm
N_d^+	ionized donor atom density (cm^{-3})
N_a^-	ionized acceptor atom density (cm^{-3})
N_{dop}	net local dopant concentration (cm^{-3})
p	hole carrier density (cm^{-3})
q	electronic charge (C)
Q_i	charge assigned to node i (C)
Q_P	charge on a particle at point P (C)
R	carrier recombination rate ($cm^{-3} s^{-1}$)
T	temperature (K)
X	parameter used in mobility calculations in eqns (15) and (17) in text
α, β	constants used in eqns (16) and (20) in text
Δt	computational time step (s)
ϵ	silicon permittivity ($F cm^{-1}$)
ε_M	L-2 error norm
$\mu_n(\mu_p)$	effective electron (hole) mobility ($cm^2 V^{-1} s^{-1}$)
μ_L	lattice mobility ($cm^2 V^{-1} s^{-1}$)
μ_I	impurity mobility ($cm^2 V^{-1} s^{-1}$)
μ_{ccs}	carrier–carrier scattering mobility ($cm^2 V^{-1} s^{-1}$)
$\rho(r,z)$	net charge density at coordinates (r,z) ($C cm^{-3}$)
$\tau_n(\tau_p)$	electron (hole) lifetime (s)
ϕ	electrostatic potential (V)
Φ_i	potential at node i (V)
$\Phi_{t,i}^M$	potential at node i and time t, for time step Δt^M
χ	dimensionless distance used in eqn (24) in text

1. INTRODUCTION

Application of particle simulation (PS) methods to semiconductor devices was reported by Hockney et al. in 1974[1]. Their approach was an extension of previous simulations of plasmas, in which the entire collection of charged particles within the plasma is represented by a computationally reasonable number of particles. Hockney et al. simulated the steady-state operation of GaAs and silicon FETs and diodes using 12,000–30,000 particles, using either a full Monte Carlo transport scheme or the static-mobility diffusion approximation (SMDA) in which a particle's motion consists of a drift and a diffusive component. They employed a uniform mesh to permit the use of fast Fourier transform (FFT) techniques to solve for the potential profile. A review of this PS/FFT approach to device analysis is presented in a book by Hockney and Eastwood[2].

A number of authors have applied particle methods to device simulation since that work. As a few examples, Pone et al. analyzed GaAs FETs using PS and SMDA methods[3], Lippens et al. analyzed millimeter-wave IMPATT devices using PS and SMDA methods[4], and Moglestue employed Monte Carlo particle methods to analyze GaAs MESFETs[5]. Use of PS methods is attractive because of the convenience with which Monte Carlo transport methods can be implemented.

Although PS methods in device analysis have been refined since their introduction, they remain fundamentally unchanged. Many of the above-

mentioned applications rely on FFT solutions of Poisson's equation developed by Hockney *et al.* Although FFT analysis permits a major speedup in potential calculations, complex device geometries are more difficult to simulate and internal electrodes require additional computations involving capacitance matrix methods[2]. The requirement of regularly spaced meshes and the difficulty of treating irregular device geometries has tended to discourage widespread use of the FFT method. More general solution methods based on non-FFT finite-difference techniques can become computationally prohibitive. Apparently PS methods have not been extended for use with numerical techniques other than finite difference techniques, and only majority carrier transport has been simulated.

Our approach merges these PS methods with a finite element (FE) solution of Poisson's equation, to allow more flexibility in device geometries and nonuniform meshes. To avoid discontinuities of electric field across inter-element boundaries, we have used quadratic interpolation of potential and density rather than the linear interpolation typically used in FE device analyses. A major goal of our work is the simulation of transient charge collection from cosmic ion tracks in semiconductor microcomponents. To approximate three-dimensional (3-D) analyses of charge collection, we have taken advantage of the axisymmetric nature of charge tracks to employ an axisymmetric FE formulation for the solution of Poisson's equation. We initially use the simpler drift-diffusion model of carrier transport, although Monte Carlo particle transport can be readily implemented in the future.

In the next section we introduce our hybrid FE/PS method, then we formulate the axisymmetric FE solution of Poisson's equation (Section 3) and discuss the particle model (Section 4). Results are presented for 1-D and axisymmetric silicon diodes in Section 5. Finally, conclusions of this work are discussed in Section 6.

2. THE HYBRID FINITE-ELEMENT/PARTICLE-SIMULATION METHOD

The differential equations governing device behavior are Poisson's equation and the electron and hole continuity equations:

$$\nabla \cdot \epsilon \nabla \phi = -q(p - n + N_d^+ - N_a^-) \qquad (1)$$

$$\frac{\partial n}{\partial t} = \frac{1}{q} \nabla \cdot \mathbf{J}_n + (G - R) \qquad (2)$$

$$\frac{\partial p}{\partial t} = -\frac{1}{q} \nabla \cdot \mathbf{J}_p + (G - R) \qquad (3)$$

plus the related current-density equations:

$$\mathbf{J}_n = qn\mu_n \mathbf{E} + qD_n \nabla n \qquad (4)$$

$$\mathbf{J}_p = qp\mu_p \mathbf{E} - qD_p \nabla p \qquad (5)$$

in which ϵ is the material permittivity, ϕ the potential, n and p the electron and hole densities, N_d^+ and N_a^-

the ionized donor and acceptor densities, q the electronic charge, $\mathbf{J}_n$ and $\mathbf{J}_p$ the electron and hole current densities, $(G - R)$ the net generation/recombination rate, μ the mobility, D the diffusivity, and $\mathbf{E}$ the electric field. Coupling between these equations typically requires either the Newton–Raphson iteration scheme for simulaneous solution of ϕ, n and p, or an iterative technique in which Poisson's equation and the continuity equations are alternatively solved until the desired accuracy is obtained for each time step. When the governing equations are strongly coupled (e.g. in transient simulations), the Newton–Raphson method is typically required although at a cost of large matrix inversions.

The use of particle methods to represent the current continuity equations allows decoupling of these equations from Poisson's equation, permitting consecutive evaluation of the particle-pushing and potential solution steps at each time step. This approach allows accurate treatment of transient device conditions if the time step and mesh sizes used are appropriately determined for convergence within the time step, and the mobility accurately approximates the scattering mechanisms involved. The complexity of matrix manipulations is also reduced, with only the solution of Poisson's equation requiring matrix evaluations.

The use of FE methods for device simulation has become well established after its introduction by Hachtel *et al.*[6] and popularization by Barnes and Lomax[7]. We chose the FE method for solving Poisson's equation because of convenient similarities with PS methods, such as the use of the same shape functions for interpolation of potential from the mesh nodes across the triangular elements as are used in the particle-to-mesh charge weighting and mesh-to-particle force interpolations required by particle methods. Evaluation of the local shape functions at the particle's position also provides a convenient means of locating the particle within specific elements after the particle-pushing step.

Although linear interpolation of potential across a triangular element is much simpler than quadratic interpolation (i.e. requiring three nodes per element vs six), the resulting discontinuities in the force on particles crossing inter-element boundaries generates increased computational noise in the system. To avoid this, we chose to use quadratic interpolation of potential to maintain continuity of force across element boundaries. Although more complicated, such a formulation permits larger element sizes for similar accuracy compared with the linear interpolation. Our interest in simulating charge collection from heavy ion tracks in semiconductor devices encouraged us to formulate Poisson's equation in axisymmetric geometry, to approximate 3-D device effects at reduced computational requirements but without the oversimplification obtained by 2-D simulations of charge track evolution.

3. AXISYMMETRIC QUADRATIC FINITE-ELEMENT FORMULATION

In the axisymmetric formulation, each element represents a 3-D triangular ring around the axis of symmetry of the device. We use triangular elements because they more easily approximate irregular boundary regions and interfaces. In our formulation, the exact solution ϕ to Poisson's equation is approximated by a quadratic interpolating function defined over each element:

$$\phi \approx N_1 \Phi_1 + N_2 \Phi_2 + , \cdots , + N_6 \Phi_6 \qquad (6)$$

with Φ_i the value of the potential at each node i of the element and N_i the nodal shape functions of magnitude 1 at node i and 0 at all other surrounding nodes. The concepts of local and global shape functions should be clarified. For linear interpolation using three nodes per triangle, the local shape functions L_i and the global shape functions N_i are identical. For quadratic interpolation, the six global shape functions N_i are quadratic with respect to the three local shape functions L_i (i.e. of order L_i^2).

Typical FE formulations of Poisson's equation employ either the variational or Galerkin approaches (see e.g. [7] and [8]). Governing equations were derived for both approaches, but the Galerkin method was found to give simpler governing equations (i.e. with lower powers of the local shape functions) and was thus employed in our formulation[9].

In the Galerkin method, each side of Poisson's equation [eqn (1)] is weighted by the shape function N_j, and that product integrated over the region to be modeled. In axisymmetric cylindrical coordinates the governing equation becomes:

$$\int_V N_j \left[\frac{1}{r} \frac{\partial}{\partial r} \left(r \frac{\partial \phi}{\partial r} \right) + \frac{\partial^2 \phi}{\partial z^2} \right] dV$$
$$= -\frac{1}{\epsilon} \int_V N_j \rho(r,z) \, dV \qquad (7)$$

in which $\rho(r,z) = -q(p - n + N_d^+ - N_a^-)$, and the assumption of an isotropic dielectric constant has been made. The volume element dV equals $2\pi r \, dr \, dz$. The region is broken up into a collection of triangular elements.

To evaluate spatial derivatives of the interpolating function, we note that N_i is a function of r and z, while Φ_i has a specified value only at the node i and is zero elsewhere. With the integral now evaluated over the region of a single element, eqn (7) takes the form:

$$\sum_{i=1}^{6} \left(\int_{V^e} \left\{ N_j \left[\frac{1}{r} \frac{\partial}{\partial r} \left(r \frac{\partial N_i}{\partial r} \right) + \frac{\partial^2 N_i}{\partial z^2} \right] \right\} dV \right) \Phi_i$$
$$= -\frac{1}{\epsilon} \int_{V^e} N_j \rho(r,z) \, dV. \qquad (8)$$

This generates the matrix equation for the element:

$$[k^e]\{\Phi\} = \{f^e\} \qquad (9)$$

As the integral term on the left-hand side of eqn (8) corresponds to $N_j \nabla^2 N_i$ in cylindrical coordinates, the first form of Green's theorem gives:

$$k_{ij} = \int_{V^e} N_j \nabla^2 N_i \, dV = -\int_{V^e} \nabla N_j \cdot \nabla N_i \, dV$$
$$+ \int_{S^e} N_j \nabla N_i \cdot \mathbf{n} \, dS \qquad (10)$$

with $\mathbf{n}$ the unit vector normal to the surface enclosing the region V^e. The surface term equals zero for common semiconductor device boundary conditions (i.e. Dirichlet boundary conditions with ohmic contacts, or Neumann boundary conditions at planes of symmetry or typical semiconductor/insulator interfaces) so eqn (10) becomes:

$$k_{ij} = \int_{V^e} \left[\frac{\partial N_j}{\partial r} \frac{\partial N_i}{\partial r} + \frac{\partial N_j}{\partial z} \frac{\partial N_i}{\partial z} \right] r \, dr \, dz. \qquad (11)$$

In eqn (8), $\rho(r,z)$ must also be interpolated from the same nodes at which the potential is evaluated, i.e. $\rho(r,z)$ is expressed analogously to ϕ in eqn (6).

The integrals for k_{ij} and f_i are too involved to evaluate analytically, so we use Gaussian quadrature. All terms in eqn (11) are converted into functions of the local shape functions L_1, L_2 and L_3, and Gaussian quadrature is applied to local L-space.

As k_{ij} and f_i are evaluated element-by-element, they are combined into an overall matrix equation with the unknown potentials Φ_i at each node:

$$[K]\{\Phi\} = \{F\} \qquad (12)$$

with $[K]$ an $m \times m$ banded symmetric matrix and $\{\Phi\}$ and $\{F\}$ column vectors of length m, with m the total number of nodes.

Prior to solution for $\{\Phi\}$, any Φ_i specified by Dirichlet boundary conditions (e.g. at ohmic contacts) are imposed on the system of eqn (12) by standard techniques. For our problem, the Choleski LU decomposition of the banded symmetric matrix $[K]$ is efficiently used to solve for Φ_i. We use IMSL routines LEQ1PB for initial inversion of the K-matrix and LUELPB for subsequent solutions of Φ_i at each time step[10]. Although this method may be more time consuming than some iterative matrix solution methods, no convergence problems are expected.

4. PARTICLE MODEL

Particle-simulation methods typically use a rectangular grid. The nearest-grid-point (NGP) and cloud-in-cell (CIC) methods are commonly used to allocate charge to nearby grid points for potential field calculations. The NGP method assigns the entire charge of a particle to the nearest grid point, but the amount of inherent computational noise can be significant as the moving particle's charge discontinuously jumps from one grid point to the next. Instead, CIC allocates the charge of the particle to several

nearby grid points, in effect extending the particle from a point charge to a cloud of charge. With our irregularly shaped triangular mesh, we use the same quadratic shape functions [eqn (6)] to assign charge from particle to nodes. The charge Q_i assigned to node i from a particle at point P is given by:

$$Q_i = N_i Q_P. \qquad (13)$$

With the charge allocated to the nodes, Poisson's equation is solved for the nodal potentials. In interpolating the nodal potentials Φ_i back to the particle positions, the electric field at a point is given by:

$$\mathbf{E} = -\nabla\phi = -\left[\sum_{i=1}^{6} \Phi_i \frac{\partial N_i}{\partial r} \mathbf{r} + \sum_{i=1}^{6} \Phi_i \frac{\partial N_i}{\partial z} \mathbf{z}\right]. \qquad (14)$$

We know the spatial derivatives for each value of i in terms of the local shape functions L_i and have previously calculated the values of L_1, L_2 and L_3 for each particle's position, so we can calculate the force on the particle directly.

The particles are advanced in position over each time step using one of two methods. The simpler SMDA method (drift-diffusion model) considers each increment in particle position to be composed of two components, one due to the electric-field-induced drift of electrons (of magnitude $\mu \mathbf{E} \Delta t$ with Δt the time step) and the other due to a random diffusional motion [of magnitude $(4D \Delta t)^{1/2}$][1]. This approach assumes the carrier velocities are instantaneously related to the field by a field-dependent mobility, as in conventional device simulation codes such as PISCES[11]. The second method is a complete Monte Carlo (MC) treatment, where rates of scattering are evaluated for all relevant scattering mechanisms. Although the MC method more accurately treated nonequilibrium transport, Hockney et al. report that the MC approach can be 10 times more expensive in computer time than SMDA[1]. As we are initially emphasizing silicon device simulations, we have implemented the SMDA transport method for all particles as a good approximation.

We evaluate the mobility using a calculation procedure proposed by Dorkel and Leturcq[12]. The carrier mobility is calculated as:

$$\mu = \mu_L \left[\frac{1.025}{1 + \left(\dfrac{X}{1.68}\right)^{1.43}} - 0.025\right] \qquad (15)$$

with μ_L the lattice mobility given by:

$$\mu_L = \mu_{L_0} \left(\frac{T}{300}\right)^{-\alpha} \qquad (16)$$

in which T is the temperature and μ_{L_0} and α are parameters dependent on the type of carrier and the temperature range. In eqn (15), X is given by:

$$X = \sqrt{\frac{6\mu_L(\mu_I + \mu_{ccs})}{\mu_I \mu_{ccs}}} \qquad (17)$$

with μ_I the impurity mobility and μ_{ccs} the carrier-carrier scattering mobility given by:

$$\mu_I = \frac{AT^{3/2}}{N_{dop}} \left[\ln\left(1 + \frac{BT^2}{N_{dop}}\right) - \frac{BT^2}{N_{dop} + BT^2}\right]^{-1} \qquad (18)$$

$$\mu_{ccs} = \frac{2 \times 10^{17} T^{3/2}}{\sqrt{np}} \{\ln[1 + 8.28 \times 10^8 T^2(np)^{-1/3}]\}^{-1}. \qquad (19)$$

In eqn (18), N_{dop} is the net local dopant concentration and A and B are carrier-dependent parameters. In eqn (19), n and p are respectively the electron and hole carrier concentrations. The above expressions are appropriate for weak-electric-field conditions. Extension to situations involving strong electric fields uses an approach suggested by Caughey and Thomas[13]:

$$\mu = \frac{\mu_0}{\left[1 + \left(\dfrac{E}{E_c}\right)^{\beta}\right]^{1/\beta}} \qquad (20)$$

in which E is the magnitude of the local electric field, E_c is a carrier-dependent constant, and μ_0 is the result from eqn (15). The constants used in eqns (15)–(20) are given in Table 1. The diffusivities D_n and D_p are obtained from eqn (20) using the Einstein relation.

Minority carrier transport is handled simultaneously with the majority carriers. The np-product is used as a measure of the relative carrier recombination or thermal generation during each time step, after nodal carrier densities are evaluated and before the solution of Poisson's equation. The net rate of carrier thermal generation and recombination is given by the standard expressions for Shockley–Read-Hall and Auger recombination[14]:

$$G - R = (n_{int}^2 - np)\{[\tau_n(p + n_{int}) + \tau_p(n + n_{int})]^{-1} + c_n n + c_p p\} \qquad (21)$$

with the local carrier lifetimes given by:

$$\tau_n = \frac{3.95 \times 10^{-5}}{1 + \left(\dfrac{N_{dop}}{7.1 \times 10^{15}}\right)} s \qquad (22)$$

$$\tau_p = \frac{3.52 \times 10^{-5}}{1 + \left(\dfrac{N_{dop}}{7.1 \times 10^{15}}\right)} s \qquad (23)$$

with n_{int} the intrinsic carrier density and the Auger coefficients $c_n = 2.8 \times 10^{-31}$ cm^6/s and $c_p = 9.9 \times 10^{-32}$ cm^6/s.

Table 1. Constants used in mobility calculations

Constant	Electrons	Holes
T(K)	300	300
μ_{L_0}(cm^2 V^{-1} s^{-1})	1430	495
α	2.2	2.2
A(cm^{-1} V^{-1} s^{-1} K$^{-3/2}$)	4.61×10^{17}	1.0×10^{17}
B(cm^{-3} K^{-2})	1.52×10^{15}	6.25×10^{14}
E_c(V cm^{-1})	8000	19,500
β	2	1

The only boundary conditions imposed on the particles are those required by equilibrium conditions at the ohmic contacts. After each time step, the majority carrier density within the contact boundary elements is equilibrated to match the doping density, and the minority carrier density is adjusted to satisfy the thermal equilibrium condition at the contact (i.e. $n_{int}^2 = np$).

The total number of particles increases after each time step to maintain equilibrium densities at the contacts and to simulate thermal generation. The magnitude of local charge generation and recombination is determined by the free carrier densities within the region around each node. The particles surrounding each node are tabulated, and their charges are adjusted to reflect generation and recombination. If the charge adjustment would be greater than, e.g. 50% per particle, additional particles are created to maintain the necessary charge balance. Charge reduction is preferentially applied to the neighboring particles with the largest charge, and generation to the particles with smaller charges.

To prevent unlimited increase in the total number of particles, particle reformulation is implemented when a specified number is exceeded. Typically a variation in total particle number of 25–50% is permitted. The total number is reduced according to some average number of particles per element, with heavier-doped elements permitted a larger number. Particles are randomly killed off and their charge transferred to neighboring particles. After reformulation, all particles of the same polarity within each element have the same average charge. For particles moving from heavily to lightly doped regions, this periodic reformulation redistributes the charge from a larger particle to the smaller neighboring particles. Only a small fraction of particles moves into neighboring elements during each time step, so with reformulation frequencies of 5–10% or more, this periodic reformulation accompanied by generation/ recombination charge adjustment effectively smooths out the particle-to-particle charge fluctuations inherent in transport between regions of varying doping. Conservation of charge is maintained at all times during particle reformulation.

5. RESULTS

One-dimensional benchmark computations were performed on a 3-V reverse-biased silicon diode with 10^{15} cm^{-3} doping density on each side of an abrupt junction (i.e. no doping variation in the radial direction). The depletion zone was allowed to evolve to steady state. The resulting potential and electric field profiles were compared to the analytical solutions for an abrupt pn junction[15] and found to be in very good agreement as documented in Ref. [9]. These low doping levels permit simpler analyses in the verification of our method than do densities approaching degenerate conditions.

For more rigorous benchmarking, the results of this FE/PS method are compared to a finite-element solution based on the Newton–Raphson iteration of the coupled current continuity and Poisson equations until a self-consistent steady state is achieved[16]. A one-dimensional case is simulated, with the device schematic shown in Fig. 1: a 3-V reverse-biased pn junction with 10^{15} cm^{-3} doping is allowed to evolve to steady state, and the results compared to the steady-state potential and carrier profiles obtained from the self-consistent device simulation code. Figure 2(a) shows the electron density profiles evolving in time, Fig. 2(b) the hole density profiles, and Fig. 2(c) the potential profiles. With the abrupt junction at 3 μm, Fig. 2(a) and (b) shows initial diffusion of the majority carriers across the junction, but as time proceeds the depletion zone forms and steady-state profiles are obtained, in good agreement with the benchmark calculations provided by the iterative self-consistent code.

Very good quantitative agreement between the two codes is obtained for majority carrier profiles and effective depletion widths. Minority carrier profiles show some variation, but these are not significant for realistic device modeling. The computational noise apparent in the density profiles is inherent in the particle method. An average of 15 particles each for positive and negative charge per element were used in this simulation. Simulations using half this average number showed no significant difference in the overall profiles, but slightly more noise in the density profiles. Although quadratic interpolation of carrier densities is used in the Poisson solution, the densities in Fig. 2(a) and (b) are represented by linear interpolation to the corner nodes. We determined that
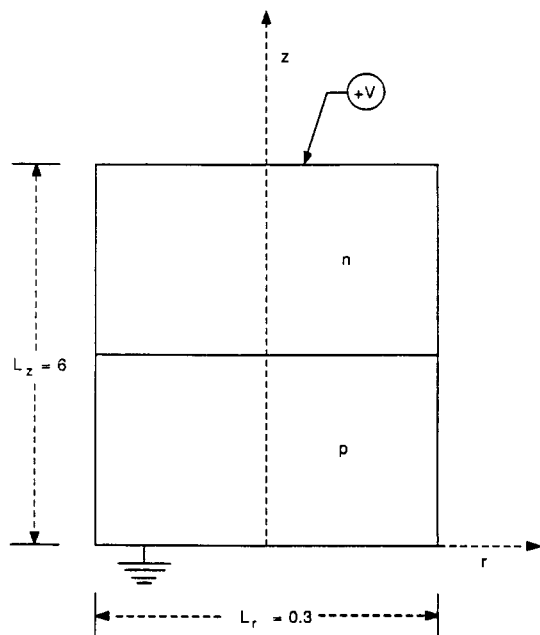

Fig. 1. Axisymmetric 1-D device simulation showing the geometry of the reverse-biased silicon diode $(V = 3$ V, geometry units are in μm).
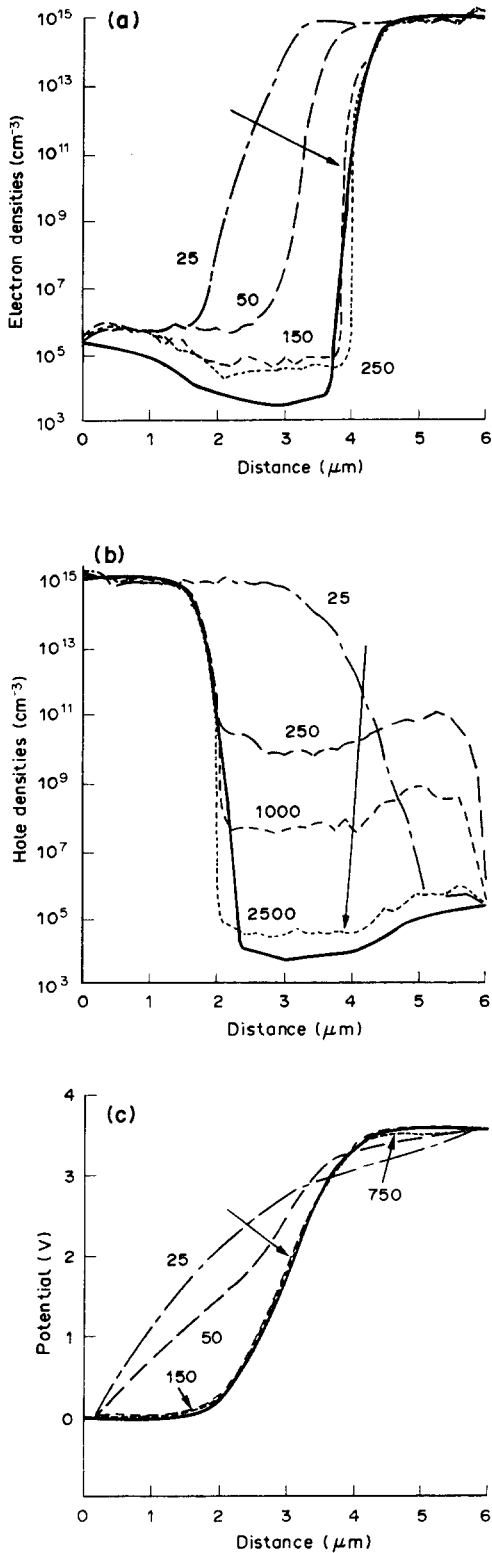
quadratic visualization of the densities (six nodes per triangle) showed systematic oscillations at non-corner nodes.

Figure 2(c) also shows very good agreement between the steady-state potential profiles obtained by the two codes. The PS code offers the advantage of observing the transient evolution of the device toward steady state. Because of large electron mobilities, the electron density profiles for these low doping levels quickly approach steady state within 0.25 ns. The lower hole mobilities prevent hole density profiles from approaching steady state for a few ns; the minority carrier hole profiles gradually decline due to drift, diffusion, and recombination. Figure 2(c) shows the potential distribution approaches steady state on a time scale comparable to that of the electron distribution.

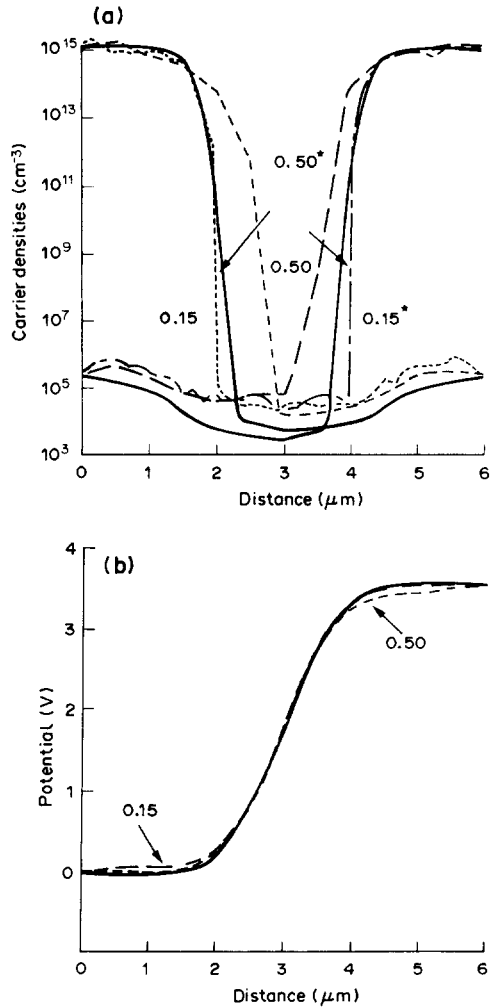Figure 3(a) and (b) shows carrier density and potential profiles at steady state for fine and course

Fig. 2. Evolution of density and potential profiles with time, after applying reverse-bias to the 1-D silicon diode. The FE/PS code results (at times given in ps) for (a) electron and (b) hole carrier densities, and (c) potential profile. The solid lines give steady-state results from iterative self-consistent FE code. Arrows indicate direction of profile evolution with time.

Fig. 3. Effect of grid element size (in μm) on steady-state profiles, showing FE/PS code results at 2.5 ns for (a) electron (✱) and hole carrier densities (arrows indicate change from coarse to fine grid) and (b) potential profiles. The solid lines show steady-state results from iterative self-consistent FE code.

grids, compared to the benchmark calculations of the iterative code. The profiles obtained by the FE/PS code using a fine mesh (0.15 μm element size, 0.075 μm between mesh points) show very good agreement with the self-consistent code. Surprisingly, even the profiles obtained using a very course mesh (0.25 μm between mesh points) are in good qualitative agreement for carrier densities and close to quantitative agreement for potential profiles. These results suggest that the quadratic FE formulation reduces the restrictions on small mesh spacings as suggested for typical device simulations[11].

Figure 4(a) and (b) shows the steady-state results for a more typical silicon diode, with n^+-region doping densities of 10^{17} cm^{-3} and p-region doping of 10^{15} cm^{-3}. Also shown are the results of the self-

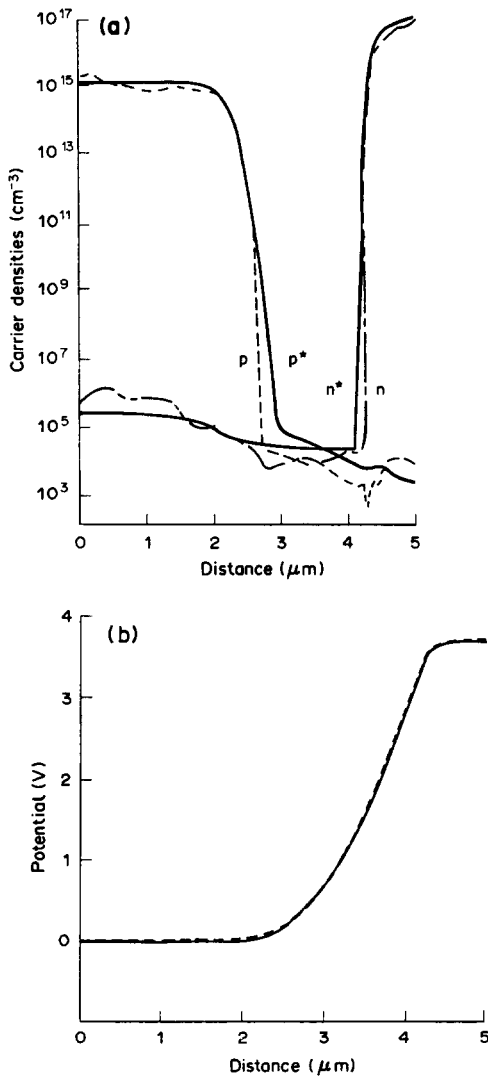consistent code. The average number of majority carrier particles per element is increased 10-fold within the n^+-region to accommodate the 100-fold increase in doping density. The doping profile does not assume an abrupt junction, but rather employs an analytical doping expression previously used in another simulation to better represent a graded junction[17]:

$$N_d^+ - N_a^- = 1.01 \times 10^{17} \exp[-116.54(1 - \chi^2)]$$
$$- 1 \times 10^{15} \text{cm}^{-3} \quad (24)$$

where χ is a dimensionless distance across the device (0.0 at the p-region contact, 1.0 at the n^+-contact, and 0.8 at the junction for this 5 μm device). The use of this doping profile is more realistic than an abrupt junction, and also reduces the computational difficulties inherent in a discontinuous order-of-magnitude change in doping densities across the junction.

These simulations use time steps of 5×10^{-14} s for initial device evolution. The time step, Δt, is subsequently increased to 10^{-13} s for heavier doping and 5×10^{-13} s for light doping conditions. Other particle simulations often use Δt of 5×10^{-14} s[1, 3, 4]. As a means of evaluating the self-consistent accuracy of these transient calculations and providing a check on the values of Δt used, the L-2 error norm was applied to the transient evolution of the above device with doping of 10^{17}–10^{15} cm^{-3}. The potential values at the mesh points were compared at 25.6-ps intervals to a second transient calculation which used twice the Δt, over a total of 256 ps. The time step was varied from 0.8 to 0.025 ps. The relative error in potential values for each pair of time steps was calculated by:

$$\varepsilon_M = \frac{1}{N_t N_x} \sqrt{\sum_t \sum_i \left(\frac{\Phi_{t,i}^{M-1} - \Phi_{t,i}^M}{\Phi_{max}}\right)^2}, \quad (25)$$

with $\Phi_{t,i}^{M-1}$ and $\Phi_{t,i}^M$ the potentials at node i and time t (with Δt^{M-1} twice that of Δt^M), Φ_{max} the applied potential across the device, and N_t and N_x the number of time intervals and grid points used in the comparison, respectively. Figure 5 shows the results of these comparisons for each Δt^M. The reduced variation in

Fig. 4. Steady-state profiles for 3-V reverse-bias, 5-μm silicon diode with n^+ doping of 10^{17} cm^{-3} and p doping of 10^{15} cm^{-3}, showing (a) FE/PS code results at 900 ps for electron (n) and hole (p) densities and iterative FE code results (n^* and p^*); and (b) potential profiles for FE/PS (– – –) and iterative FE (——) codes.
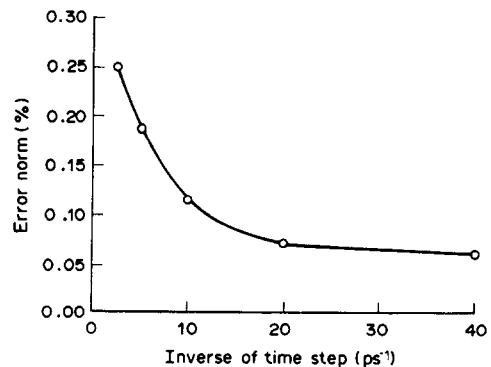

Fig. 5. Reduction in L-2 error norm as a function of the time step Δt. Each point represents the relative difference in the nodal potentials between calculations with the specified Δt and a time step of $2\Delta t$.
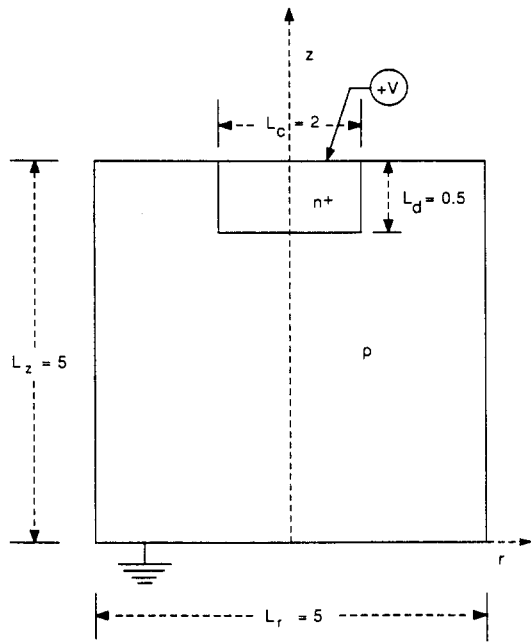
Fig. 6. Axisymmetric device simulation showing geometry of the reverse-biased silicon diode ($V = 3$ V, geometry units are in μm).

potential for decreasing Δt demonstrates self-consistency of the transient results. The saturation in error norm reduction as Δt approaches 0.05–0.025 ps supports our use of 0.05 ps, with tolerable error for Δt of 0.1 ps under heavy doping conditions.

Figures 6 and 7 demonstrate the axisymmetric capabilities of our code, with an n^+-region doping of 10^{17} cm^{-3} and a p-region doping of 10^{15} cm^{-3}. A schematic of the silicon device simulated is shown in Fig. 6; Because of symmetry only half of the device is modeled. Figure 7(a) and (b) shows the electron density and potential profiles near steady state (after 350 ps of device evolution). These profiles compare favorably with previous simulations using similar device conditions and geometry (see e.g. [17]).

Computational details of the above simulations are provided in Table 2. All calculations were performed on a CRAY-2 computer. The bandwidth of the governing matrix equation strongly impacts the solution time for Poisson's equation. The code has not been optimized, and the CPU times include
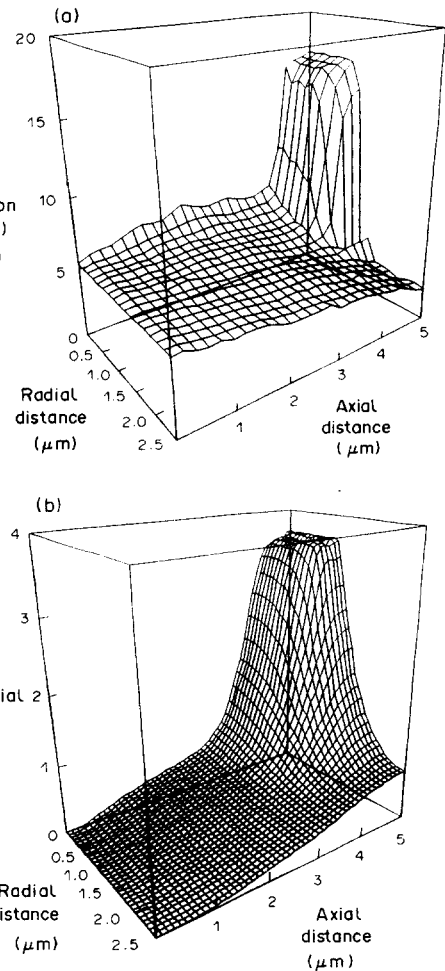

Fig. 7. Axisymmetric device simulation after 350 ps showing (a) electron density and (b) potential profiles.

significant effort in post-processing and graphical computations.

6. CONCLUSIONS

(1) A hybrid numerical method combining particle simulation and finite-element methods has been developed which compares well with traditional finite-element solution methods. The use of quadratic finite-element interpolation relaxes the restriction on maximum element size.

Table 2. Computational details

Doping (cm^{-3})	Number of elements	Element size (μm)	Band width	Time step (ps)	Number of timesteps	Simulation time (ns)	Maximum No. of particles	CPU time (min)
$\pm 10^{15}$	24	0.50 × 0.15	7	0.05 – 0.5	6500	2.5	579	2.9
$\pm 10^{15}$	40	0.30 × 0.15	7	0.05 – 0.5	6500	2.5	918	4.7
$\pm 10^{15}$	80	0.15 × 0.15	7	0.05 – 0.5	6500	2.5	1769	9.2
-10^{17} $+10^{15}$	70	0.075 – 0.20	7	0.05 – 0.5	3300	0.9	6320	11.9
-10^{17} $+10^{15}$	800	0.10 – 0.25	103	0.05 – 0.1	3500	0.325	6755	26.9
-10^{17} $+10^{15}$	800	0.10 – 0.25	103	0.05	500	0.025	24,151	10.1

Computations performed on a CRAY-2 computer.

(2) Unlike previous uses of particle methods, this numerical method accurately simulates both majority and minority carrier transport simultaneously.

(3) The method offers versatility in the simulation of transient device conditions and potential for studying the physics of nonequilibrium transport.

(4) The method shows promise for further studies of fast transients such as the collection of charge from ion tracks in semiconductors.

REFERENCES

1. R. W. Hockney, R. A. Warriner and M. Reiser, *Electron. Lett.* **10**, 484 (1974).
2. R. W. Hockney and J. W. Eastwood, *Computer Simulation Using Particles*. McGraw-Hill, New York (1981).
3. J.-F. Pone, R. C. Castagné, and C. Arnodo, *IEEE Trans. Electron Devices* **ED-29**, 1244 (1982).
4. D. Lippens, J.-L. Nieruchalski and E. Constant, *IEEE Trans. Electron Devices* **ED-32**, 2269 (1985).
5. C. Moglestue, *IEEE Trans. Computer-Aided Design* **CAD-5**, 326 (1986).
6. G. D. Hachtel, M. Mack and R. R. O'Brien, *Conf. Rec., Eighth Asilomar Conf. Circuits, Systems and Computers*, p. 332, Pacific Grove, CA (1974).
7. J. J. Barnes and R. J. Lomax, *IEEE Trans. Electron Devices* **ED-24**, 1082 (1977).
8. T. Adachi, A. Yoshii and T. Sudo, *IEEE Trans. Electron Devices* **ED-26**, 1026 (1979).
9. R. C. Martin and N. M. Ghoniem, University of California at Los Angeles, Report no. UCLA-ENG-8835/PPG-1195 (1988).
10. *The IMSL Library Reference Manual*, Vol. 2, 9th edn. IMSL Inc., Houston, TX (1982).
11. M. R. Pinto, C. S. Rafferty and R. W. Dutton, *PISCES II: Poisson and Continuity Equation Solver*. Stanford Electronics Laboratories, Stanford University, CA (1984).
12. J. M. Dorkel and Ph. Leturcq, *Solid-St. Electron.* **24**, 821 (1981).
13. D. M. Caughey and R. E. Thomas, *Proc. IEEE* **55**, 2192 (1967).
14. S. Selberherr, *Microelectron. Reliab.* **24**, 225 (1984).
15. J. P. McKelvey, *Solid State and Semiconductor Physics*, Chap. 12. Harper & Row, New York (1966).
16. S. P. Chou and N. M. Ghoniem, University of California at Los Angeles, Report no. UCLA-ENG-8834/PPG-1194 (1988).
17. J. P. Kreskovsky and H. L. Grubin, *J. Comput. Phys.* **68**, 420 (1987).